Atmospheric Environment 193 (2018) 302–315

Contents lists available at ScienceDirect

Atmospheric Environment

journal homepage: www.elsevier.com/locate/atmosenv

Combining model projections with site-level observations to estimate changes in distributions and seasonality of ozone in surface air over the U.S.A.

Harald E. Rieder[a,b,*], Arlene M. Fiore[b,c], Olivia E. Clifton[b,c], Gustavo Correa[b], Larry W. Horowitz[d], Vaishali Naik[d]

[a] Wegener Center for Climate and Global Change and IGAM/Institute of Physics, University of Graz, Austria
[b] Lamont-Doherty Earth Observatory of Columbia University, Palisades, NY, USA
[c] Department of Earth and Environmental Sciences, Columbia University, New York, NY, USA
[d] Geophysical Fluid Dynamics Laboratory, National Oceanic and Atmospheric Administration, Princeton, NJ, USA

ARTICLE INFO

Keywords:
Surface ozone
Ozone precursor emissions
Climate change
Representative concentration pathways
Methane
Seasonality

ABSTRACT

While compliance with air quality standards is evaluated at individual monitoring stations, projections of future ambient air quality for global climate and emission scenarios often rely on coarse resolution models. We describe a statistical transfer approach that bridges the spatial gap between air quality projections, averaged over four broad U.S. regions, from a global chemistry-climate model and the local level (at specific U.S. CASTNet sites). Our site-level projections are intended as a line of evidence in planning for possible futures rather than the sole basis for policy decisions. We use a set of transient sensitivity simulations (2006–2100) from the Geophysical Fluid Dynamics Laboratory (GFDL) chemistry-climate model CM3, designed to isolate the effects of changes in anthropogenic ozone (O_3) precursor emissions, climate warming, and global background CH_4 on surface O_3. We find that surface maximum daily 8-h average (MDA8) O_3 increases despite constant precursor emissions in a warmer climate during summer, particularly in the low tail of the MDA8 O_3 distribution for the Northeastern U.S., while MDA8 O_3 decreases slightly throughout the distribution over the West and Southeast during summer and fall. Under scenarios in which non-methane O_3 precursors decline as climate warms (RCP4.5 and RCP8.5), summertime MDA8 O_3 decreases with NO_x emissions, most strongly in the upper tail of the MDA8 O_3 distribution. In a scenario where global methane abundances roughly double over the 21st century (RCP8.5), winter and spring MDA8 O_3 increases, particularly in the lower tail and over the Western U.S. In this RCP8.5 scenario, the number of days when MDA8 O_3 exceeds 70 ppb declines in summer with NO_x emissions, but increases in spring (and winter); by the end of the century, the majority of sites in the WE and NE show probabilistic return values of the annual 4th highest MDA8 O_3 concentration above 70 ppb (the current O_3 NAAQS level). Continued increases in global CH_4 abundances can be thought of as a "methane penalty", offsetting benefits otherwise attainable by controlling non-CH_4 O_3 precursors.

1. Introduction

The U.S. National Ambient Air Quality Standard (NAAQS) for surface ozone (O_3) was revised from 84 to 75 ppb (three-year average of the 4th highest maximum daily 8-h average (MDA8)) in 2008 (Federal Register, 2008) and was again lowered to 70 ppb in 2015 (Federal Register, 2015). The NAAQS of 75 ppb has still not been attained at numerous U.S. monitoring sites, and the stricter 70 ppb standard will further expand non-attainment regions (e.g., Cooper et al., 2015; Rieder et al., 2013). Numerous studies have emphasized the potential for climate change to exacerbate ozone pollution, implying a need for tighter controls on precursor emissions to attain targeted air quality levels (e.g., recent reviews of Fiore et al., 2015; Isaksen et al., 2009; Jacob and Winner, 2009; Weaver et al., 2009; Wu et al., 2008). Below, we describe a new approach to examine a range of possible futures in light of emission and climate change scenarios at the level of the individual monitoring sites that determine compliance with the U.S. ground-level ozone standard.

In northern mid-latitude polluted regions, surface O_3 concentrations often peak during the summer season when abundant solar radiation,

* Corresponding author. Wegener Center for Climate and Global Change, University of Graz, Brandhofgasse 5, 8010, Graz, Austria.
E-mail address: harald.rieder@uni-graz.at (H.E. Rieder).

https://doi.org/10.1016/j.atmosenv.2018.07.042
Received 30 September 2017; Received in revised form 18 July 2018; Accepted 21 July 2018
Available online 25 July 2018
1352-2310/

biogenic volatile organic compounds (VOCs), and high temperature facilitate active photochemical ozone production in the presence of oxides of nitrogen (NO_x). In addition to the potential for a warmer climate to increase ozone pollution by increasing temperature-sensitive precursor emissions, kinetic reaction rates, and by changing air pollution meteorology (Barnes and Fiore, 2013; Shen et al., 2015; Steiner et al., 2006), earlier work also highlights a role for rising global methane (CH_4) abundances to raise background ozone levels including in surface air (e.g., Clifton et al., 2014; Fiore et al., 2002). Clifton et al. (2014) emphasized the potential for continued reductions in U.S. anthropogenic NO_x emissions to reverse the present-day ozone seasonal cycle over polluted regions, with a wintertime peak that can be amplified by rising global methane abundances. The applicability of archived fields from coarse resolution CCMs and CTMs to the local monitoring site level, which serves as the basis for evaluating compliance with U.S. air quality standards, is a key gap in our understanding. Here we aim to bridge this gap by harnessing the strength of a global CCM to project regional-scale changes in ground-level O_3 distributions while retaining the observed local (sub-grid) variability. Our site-level projections for surface O_3 at regionally representative sites are not intended for direct predictions but could serve as one line of evidence for policy planning.

We expand upon previous work examining surface ozone concentrations throughout the 21st century (e.g., Clifton et al., 2014; Gao et al., 2013; Pfister et al., 2014; Rieder et al., 2015; Sun et al., 2017). In particular we investigate changes across the entire MDA8 O_3 distribution throughout the 21st century and the seasonal contributions to the annual average number of days above the current 70 ppb U.S. O_3 NAAQS. As surface ozone is biased high against observations in many atmospheric chemistry models (e.g., Makar et al., 2017), we previously employed a regional quantile-mapping bias correction approach to adjust the modeled present-day concentrations in each grid cell over the Northeastern U.S. (Rieder et al., 2015). Here, we instead use projected changes at each quantile in the model, averaged over large regions, and apply these to the present-day distributions observed at each monitoring site falling within the region. We thus preserve the local variability observed at present.

We also investigate changes in the probabilistic return values of the annual 4th highest MDA8 O_3 concentration, a metric introduced in Rieder et al. (2015). The return level metric relates directly to the NAAQS, and bridges the gap to frequency-based statistics as it characterizes the offset relative to the NAAQS, by providing a quantitative context for how close the O_3 abundances are to the target level. We examine these by season, motivated by observed recent shifts in ozone seasonality and simulated changes in ozone seasonality over the 21st century in response to NO_x emission changes (Clifton et al., 2014; Parrish et al., 2013; Simon et al., 2015). With our examination of the ground-level ozone distribution across the U.S.A. by season and region, we aim to depict a broader set of potential future surface ozone pollution distributions in the contiguous U.S. under different emission and climate trajectories.

2. Model simulations, statistical approach, and evaluation

2.1. GFDL CM3 historical and future simulations and prior evaluation

We use an ensemble of RCP 21st century climate scenarios and transient sensitivity simulations (i.e., simulations with continuously varying forcings) performed with the Geophysical Fluid Dynamics Laboratory (GFDL) chemistry-climate model CM3 (e.g., Donner et al., 2011) that build from those designed for the Coupled Model Intercomparison Project - Phase 5 (CMIP5) in support of the 5th Assessment Report of the Intergovernmental Panel on Climate Change (IPCC AR5). Our configuration of CM3 applies a finite-volume dynamical core on a cubed sphere grid comprised of six faces, each with a domain of 48 × 48 horizontal grid cells (c48) and 48 vertical hybrid sigma-pressure levels extending from the surface to 0.01 hPa (~80 km), with a 70 m thick surface layer. CM3 includes fully interactive stratospheric and tropospheric chemistry and aerosols (Austin et al., 2013; Naik et al., 2013), aerosol-radiation and aerosol-cloud interactions (Donner et al., 2011; Naik et al., 2013). Tropospheric gas-phase chemistry includes reactions of NO_x-HO_x-O_x-CO-CH_4 and non-methane volatile organic compounds based on a modified version of the chemical scheme used in the Model for OZone And Related chemical Tracers version 2 (MOZART-2) (Horowitz et al., 2003, 2007).

We analyze 3 ensemble members of CMIP5 CM3 historical simulations (e.g., John et al., 2012), with anthropogenic emissions of O_3 precursors, other than methane, from Lamarque et al. (2010). Future projections follow the RCP8.5 and RCP4.5 scenarios with anthropogenic emissions of O_3 precursors from Lamarque et al. (2011); these are the same simulations, each with 3 ensemble members as in Clifton et al. (2014). Global annual mean CH_4 abundances from Meinshausen et al. (2011) are specified in the model as a lower boundary condition for chemistry calculations. Global annual mean concentrations of well-mixed greenhouse gases, including CH_4, CO_2, N_2O and stratospheric ozone depleting substances (ODS) follow the respective RCP scenario (Meinshausen et al., 2011) and from 2006 to 2100 for radiation calculations John et al. (2012). The projected CMIP5 greenhouse gas abundances, including CH_4, only consider anthropogenic changes. There are no natural methane sources feeding back in response to changes in climate in the model. Note that both RCP scenarios, RCP8.5 and RCP4.5, include sharp reductions in NO_x emissions over the U.S. during the 21st century (see Table 1 and Fig. 1a and b).

In addition to the standard GFDL CM3 CMIP5 historical, and RCP simulations, we analyze a set of sensitivity simulations from Clifton et al. (2014) to investigate the role of changes in O_3 precursor emissions, climate warming, and methane on U.S. surface ozone. Under RCP8.5_WMGG and RCP4.5_WMGG, well-mixed greenhouse gases follow the corresponding RCP scenario, but emissions of O_3 precursors and aerosols are kept constant at year 2005 levels, and methane and ODS follow the corresponding RCP scenario in the model radiation scheme, but are held at 2005 levels in the model chemistry scheme). Under the RCP8.5_WMGG scenario (Fig. 1e), annual average surface air

Table 1
Percentage changes in global abundances of CO_2 and CH_4 (treated separately for chemistry and radiation in CM3) and percentage change in anthropogenic NO_x emission (for NE, SE and WE U.S. and CA) from 2005 to 2100 in the 21st century projections used in this study.

Scenario or sensitivity simulation (# ensemble members)	global CO_2[a]	global CH_4 [a] (chemistry)	global CH_4 [a] (radiation)	NE NO_x[b]	SE NO_x[b]	WE NO_x[b]	CA NO_x[b]
RCP8.5 (3)	+147%	+111%	+111%	−83%	−83%	−58%	−84%
RCP4.5 (3)	+42%	−11%	−11%	−83%	−82%	−80%	−82%
RCP8.5_WMGG (3)	+147%	0%	+111%	0%	0%	0%	0%
RCP4.5_WMGG (3)	+42%	0%	−11%	0%	0%	0%	0%
RCP8.5_2005CH4 (1)	+147%	0%	0%	−83%	−83%	−58%	−84%
RCP8.5_2005CH4_chem (1)	+147%	0%	+111%	−83%	−83%	−58%	−84%
RCP8.5_2005CH4_rad (1)	+147%	+111%	0%	−83%	−83%	−58%	−84%

[a] from Meinshausen et al. (2011); we calculate changes relative to year 2005 CO_2 and CH_4 abundances specified per RCP.
[b] from Lamarque et al. (2011); we calculate changes relative to year 2005 NO_x emissions as specified per RCP and prescribed (per region) in CM3.

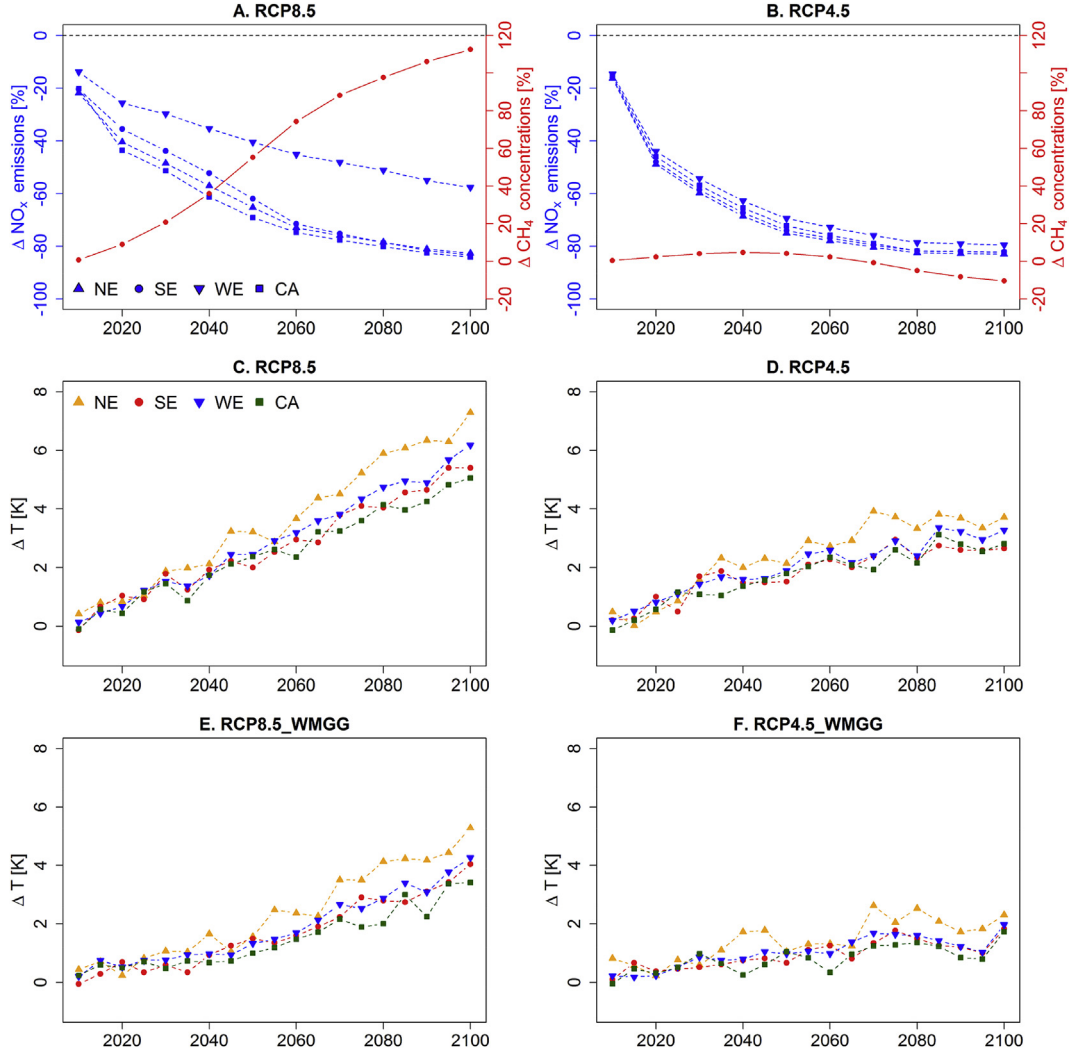

Fig. 1. Regional changes in NO_x emissions and global CH_4 concentrations during the 21st century, relative to year 2005, under the (A) RCP8.5 and (B) RCP4.5 scenarios, and regional changes in surface temperature for 5-year periods relative to 2001–2005 under the (C) RCP8.5, (D) RCP4.5, (E) RCP8.5_WMGG and (F) RCP4.5_WMGG scenarios over four U.S. regions (different symbols).

temperature increases regionally from 2001-2005 to 2096–2100 by 5.3 °C in the Northeast, 4.0 °C in the Southeast, 4.3 °C in the West and 3.4 °C in California (see definition of individual regions below, and Fig. 2a). These temperature changes are about 30% less than simulated in the full RCP8.5 scenario (Fig. 1c), which includes additional warming from reductions in aerosol emissions.

Additional sensitivity simulations allow us to investigate the influence of increasing global CH_4 abundances in RCP8.5 (approximately doubling by 2100) on surface ozone by holding CH_4 at 2005 levels (in either the chemistry or radiation scheme or in both), but allowing all other emissions and concentrations to follow RCP8.5. The regional evolution of emissions of nitrogen oxides and global mean CH_4 background abundances specified for these simulations is shown in Fig. 1a–b (note the regions are depicted in Fig. 2a).

The analysis of multi-member ensembles (five-member historical ensemble; three-member RCP4.5, RCP8.5, RCP4.5_WMGG and RCP8.5_WMGG ensembles, 1-member for RCP8.5_2005CH4) provides an opportunity to study the robustness of forced responses while providing a measure of the unforced internal variability ("noise") generated by the chaotic climate system. The 5 individual historical ensemble members (1860–2005) are launched from initial conditions separated by 50 years in the CM3 pre-industrial control simulation (perpetual 1860 conditions). The future simulations under the RCPs (and corresponding sensitivity simulations) are continuations of three of the respective historical ensemble members for the time period 2006–2100 (see Table 1).

The GFDL AM3/CM3 model has been evaluated against observations in a series of studies and shown to simulate - despite a mean state bias (e.g., Rieder et al., 2015) - plausible responses of U.S. surface ozone to emission changes, and changes in ozone seasonality over recent decades (Clifton et al., 2014; Lin et al., 2015, 2017; Rieder et al., 2015). Recent studies with the atmospheric component of this model (GFDL AM3; which in our study is coupled to full ocean and sea ice models, referred to as CM3) show that the model represents observed trends at high altitude sites, typically interpreted as measuring "baseline" air (Lin et al., 2017; see their Figs. 7–9). Specifically, Lin et al. (2017) nudge AM3 to observed meteorology (and thus force it to act as a chemistry-transport model rather than a climate model) and find that the model captures observed trends at low elevation sites (e.g., in the eastern and central U.S.A.). For the high-altitude western U.S. sites, Lin et al. (2017) filter the simulated O_3 abundances to include only those time periods when the model grid cell is actually representative of the free tropospheric air sampled by the monitors at high altitude sites (via a tagged tracer of anthropogenic carbon monoxide emitted within North America).

Along with the set of CM3 simulations, we analyze surface ozone

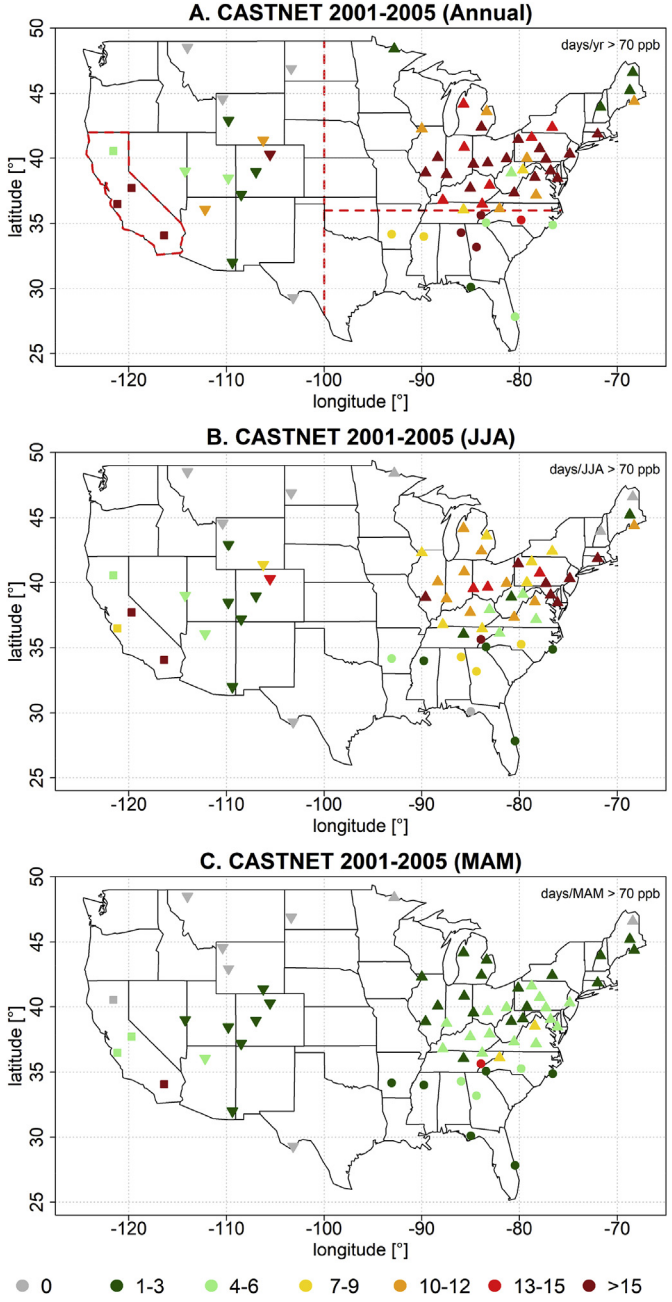

Fig. 2. Average number of days above 70 ppb at CASTNet sites in 2001–2005 for (A) annual, (B) summer (JJA), (C) spring (MAM). Symbols indicate the four regions considered: Northeast (filled upward triangles), Southeast (filled circles), West (filled downward triangles) and California (filled squares). Filling is indicative of the average number of days, binned, as indicated in the legend. Note: only CASTNet sites with more than 80% data coverage in 2001–2005 are shown. Red crosshair and red state border in panel (A) marks regional domains. Figure S1 shows these statistics for fall and winter. (For interpretation of the references to color in this figure legend, the reader is referred to the Web version of this article.)

observations from the US Environmental Protection Agency (EPA) Clean Air Status and Trends Network (CASTNet; http://www.epa.gov/castnet), which provides a regionally representative view of rural U.S. surface O_3 concentrations. In this study we use observations from 65 CASTNet sites within the contiguous U.S. that fulfill our data selection criterion of at least 80% data coverage within 2001–2005. We select the time period 2001–2005 as our reference period (see Fig. 2) because substantial regional emission controls (e.g., the NO_x State Implementation Plan in the Northeastern U.S.) were implemented starting just before this period in the late 1990s, and it comprises the last five years of the historical CM3 simulations. We note that all "future" CM3 simulations extend from 2006 to 2100. To illustrate ozone air quality over this baseline period Fig. 2a–c shows the average number of days per year (and per summer and spring season) exceeding 70 ppb (hereinafter referred to as DAYS > 70), at CASTNet sites between 2001 and 2005 (see Figure S1 for fall and winter exceedances).

We consider the impact of regional O_3 responses for different scenarios at individual CASTNet sites. We divide the U.S. first into West and East along the 100°W meridian and then further divide the Eastern U.S. along the 36°N line. The resulting four regions analyzed in this study are termed: Northeast (NE, includes all U.S. land grid cells east of 100°W and north of 36°N), Southeast (SE, includes all land grid cells east of 100°W and south of 36°N), West (WE, includes all land grid cells west of 100°W except over California) and California (CA, includes all model grid cells encompassing California). Earlier work has shown that these broad regions (domains indicated in Fig. 2a) vary coherently with respect to the month during which monthly mean ozone concentrations peak in the base-case CM3 simulation (see Figure S2 in Clifton et al. (2014)).

2.2. Statistical approach

Determining projected regional average changes in MDA8 O_3. For each grid cell within each of the four regions, we calculate the change in MDA8 O_3 at each quantile of the regional O_3 distribution within five-year intervals (ranging from 2006-2010 to 2096–2100) relative to 2001–2005 (*hist*) for each of the individual future CM3 simulations (*fut*). We first derive the MDA8 O_3 distribution at all model grid-cells (M) in the corresponding domain and then average across grid-cells (at 1%-quantile steps) to derive the combined regionally averaged probability density function (PDF) for each 5-year period. We then calculate the difference in 1% quantile steps (q) in each of the four regions (regional averages are denoted by an overbar) for each month as given in Eq. (1):

$$\Delta M_{\bar{q}} = M_{\bar{q}(fut)} - M_{\bar{q}(hist)} \quad (1)$$

Projecting site-level changes to the MDA8 O_3 distribution. Next we calculate 1% quantile steps at each CASTNet site for 2001–2005 ($O_{q(hist)}$). The future local response $O'_{q(fut)}$ is then calculated by adding the regional average change in the model at each quantile ($\Delta M_{\bar{q}}$) to the reference period (2001–2005) quantiles ($O_{q(hist)}$) at each CASTNet site in the regional domain (see equation (2) and Figure S2):

$$O'_{q(fut)} = O_{q(hist)} + \Delta M_{\bar{q}} \quad (2)$$

Our approach is intended to harness the strength of global-chemistry climate models in projecting average regional scale changes while retaining the observed local scale sub-grid variability. The skill of this technique is evaluated retrospectively below.

***Estimating days when MDA8 O_3 exceeds* 70 ppb.** For each CASTNet site, scenario, and 5-year interval we calculate the number of quantiles in $O'_{q(fut)}$ exceeding a given threshold value, here 70 ppb. The average number of days above this threshold level per month (m) in a 5-year period ($DAYS_m$), with $m = \{1,..,12\}$, is then calculated as the number of quantiles (n_q) exceeding the threshold divided by 100 (i.e. the total number of percentiles), times the number of days per month (n_{dpm}) (see Eq. (3)).

$$DAYS_m = \frac{n_q}{100} * n_{dpm} \quad (3)$$

For example, for a given site in a 5-year period where ten quantiles exceed 70 ppb in a month with $n_{dpm} = 30$ yields an average of 3 days above 70 ppb per year. We sum these monthly estimates on a seasonal basis (with seasons defined as spring (March-April-May), summer (June-July-August), fall (September-October-November) and winter

(December-January-February)) and round the resulting seasonal totals to the nearest whole number. Annual statistics are the sum over all 4 seasons. All reported statistics correspond to a 5-year average across the available ensemble members. Hereinafter all specified changes are based on significant (95% level) differences in the underlying regional PDFs.

Probabilistic MDA8 O_3 return values. While frequency statistics (e.g., $DAYS_m$ described above) provide information on (non-)attainment of the U.S. NAAQS for ozone they do not provide information on how close ozone pollution events are to the target threshold(s). The probabilistic T-year return level (RL^T), describes the probability of exceeding a threshold value x (here MDA8 O_3 in ppb) within a time window T (here 5 years). Such T-year return levels are frequently used to provide probabilistic information regarding the exceedance (in both magnitude and frequency) of a threshold of interest. In practice, estimates for RL^T are commonly provided by fitting one of the distributions comprising the family of extreme value distributions (e.g., Coles, 2001) to the observational data and deriving the RL^T of interest from the fitted distribution. We followed this approach in recent work for O_3 pollution events in the Eastern U.S. (Rieder et al., 2013, 2015).

As a return level is defined as a value that is expected to be equaled or exceeded on average once every interval of time (T), the probability that the maximum over a period of interest exceeds R^T, equates $p = 1 - (1 - 1/T)^T$. First, for each month we add the regional $\Delta M_{\bar{q}}$ for each quantile to the observed historic (2001–2005) quantiles at each CASTNet site. Second, as we are interested in the return value of the annual 4th highest MDA8 O_3 value averaged over 5-year periods, we sort all monthly quantiles at each site. We then derive the 13th highest quantile which corresponds to the probabilistic MDA8 O_3 value that on average is equaled or exceeded four times each year, if each month is equally weighted:

$$13 \approx \frac{4}{\left(\frac{z}{n_q}\right)}, \; with \; z = \frac{n_d}{n_m}, \tag{4}$$

where n_q is the number of percentiles in the distribution (= 100), and n_d and n_m are the number of days (365) and months (12) per model year, respectively. Note that our estimate for the annual 4th highest MDA8 O_3 value is conservative, through the use of 5-year periods, compared to the NAAQS formulation of a 3-year average.

2.3. Evaluation of using modeled regional averages to project changes at individual sites

We evaluate our approach of using regional MDA8 O_3 changes at each quantile projected by CM3, to project site level exceedances of O_3 with CASTNet observations backwards in time to an earlier period (1996–2000). This approach tests model skill at representing the MDA8 O_3 response to the 25% decrease in NO_x emissions (e.g., Frost et al., 2006) that occurred (and are imposed in the model) from 1996-2000 to 2001–2005. We include all CASTNet sites with at least 80% data coverage in the base (2001–2005) and evaluation (1996–2000) periods. This yields three fewer sites than in the original set of 65 sites considered for baseline characterization (see Fig. 2) and for future projections (Section 3). To hindcast site level exceedances of 70 ppb we follow the approach from Eqs. (2) and (3) except that the regional model response ($\Delta M_{\bar{q}}$) is now the difference between the baseline (2001–2005) and evaluation period (1996–2000) in the CM3 historical simulations.

Fig. 3 compares DAYS > 70 observed at each CASTNet evaluation site with our estimate projected backward in time using the regionally averaged model changes at each quantile. Correlation among observed and model-derived exceedances is high, ranging from 0.88 to 0.93. For the majority of sites our approach yields model back-projected site exceedances within ± 3 days of those observed. Significant deviations (i.e., > 10 days) exist for individual sites, particularly for annual and summertime exceedances at sites located in complex terrain (i.e., at Joshua Tree and Yosemite national park sites in CA). Our approach underestimates the absolute number of days above 70 ppb in the SE, most pronounced in summer. This SE underestimate may reflect inadequate sensitivity of ozone to isoprene-NO_x chemistry (e.g., Li et al., 2018; Mao et al., 2013; Travis et al., 2016) in CM3, suggesting that these model back-projected changes might be a conservative estimate.

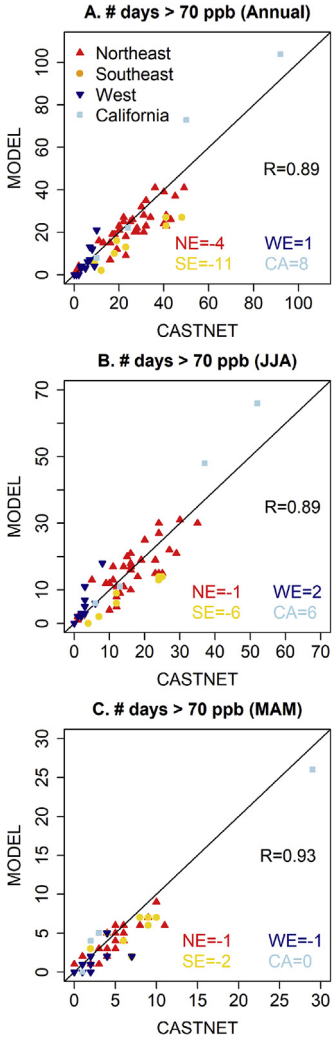

Fig. 3. Comparison of observed (CASTNet) and model simulated average number of days above 70 ppb in 1996–2000 for (A) annual, (B) summer (JJA), (C) spring (MAM). The regional mean difference in the number of days above 70 ppb between model simulations and observations is given in the bottom right corner of each panel. The black diagonal lines give the identity lines. Correlation (R) between the observed and model predicted number of days above 70 ppb is given in each panel.

3. Projecting future changes in U.S. surface ozone due to changes in NO_x emissions, climate warming and global methane

3.1. Model projected changes in regional average ozone distributions by month

Fig. 4 shows regionally averaged changes in low (10%), median (50%) and high (90%) MDA8 O_3 quantiles (hereinafter referred to as Q10 or lower tail, Q50 and Q90 or upper tail, respectively) for the early (2021–2025) and late (2096–2100) 21st century compared to 2001–2005 under RCP8.5 and sensitivity scenarios (RCP8.5_WMGG and RCP8.5_2005CH4).

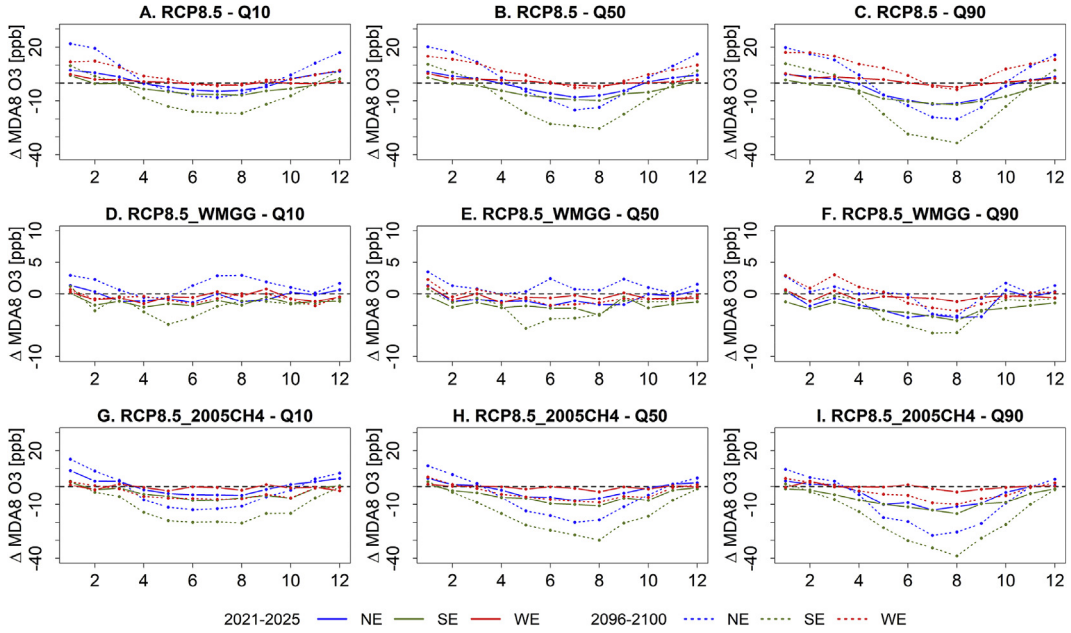

Fig. 4. Regionally 3-member ensemble averaged changes in MDA8 O_3 relative to the 2001–2005 base period as projected by CM3 for the 10%- (left column), 50%- (middle column) and 90%-quantile (right column) on a monthly basis (x-axis) under different scenarios for the early (2021–2025) and late (2096–2100) 21st century.

We focus first on the near term (2021–2025) changes in RCP8.5 (Fig. 4a–c). In the NE decreases from 2001-2005 levels in MDA8 O_3 by 2021–2025 range between −2 ppb (May and September) and −5 ppb (July) in the lower tail (Q10), −3 ppb (May) and −8 ppb (July) in the median (Q50), and −1 ppb (April) and −12 ppb (July) in the upper tail (Q90). For the SE over the same time period there are decreases between −1 ppb (November) and −7 ppb (August) in the lower tail (Q10), −1 ppb (March) and −10 ppb (August) in the median (Q50), and −2 ppb (March) and −12 ppb (August) in the upper tail (Q90). These changes result from substantial NO_x emission decreases, projected between 2005 and 2020 to reach between −35% (SE) and −40% (NE) under RCP8.5. By 2021–2025 MDA8 O_3 changes little due to climate warming (below +1 °C) and rising methane abundances (+9%).

The decreases in MDA8 O_3 grow during the 2nd half of the 21st century (Fig. 4a–c), with the largest changes occurring in the upper tail. By the end of the 21st century, decreases from the 2001–2005 base period peak in August at −33 ppb in the SE and −20 ppb in the NE. However, MDA8 O_3 increases throughout Q10, Q50 and Q90 over the 21st century during December to March in the SE, and November to April in the NE. Maximum increases, around +20 ppb, are found by 2096–2100 for January and February in the NE. For the WE MDA8 O_3 increases during winter and spring in the upper tail, reaching +17 ppb (January and February) and +15 ppb (March), respectively, by the end of the 21st century. During summer, WE U.S. changes are smaller in magnitude, negative (around −1 to −3 ppb), and largest in the high tail of the MDA8 O_3 distribution. We note that similar, though generally larger decreases and smaller increases, occur under RCP4.5 for most regions and quantiles (Figure S3).

Next we focus on changes in the RCP8.5_WMGG simulations (Fig. 4d–f), in which ozone responds only to changes in well-mixed greenhouse gases (and the resulting changes in climate). During the early 21st century (i.e., until ~ 2045) changes at low, median and high quantiles are less robust (i.e., fluctuate around ± 0 ppb) compared to RCP8.5. As time progresses, a "climate penalty" (Wu et al., 2008; the increase in ozone occurring solely because climate warmed in the absence of any changes to precursor emissions) emerges, reaching up to +4 ppb by 2100 for the NE. Results for the WE are similar to the NE (and SE) during winter and spring but differ during summer and fall when slight decreases in MDA8 O_3 occur throughout the distribution (up to 3 and 2 ppb in the upper and lower tail, respectively). This indicates that either (i) the three-member ensemble is not large enough to establish robust statistics in the context of climate variability, and/or (ii) increased ozone loss from higher water vapor in a warmer climate offsets (partly) the climate penalty. We note that some recent studies (e.g., Fiore et al., 2015; Trail et al., 2013) report also on a potential "climate benefit" such as through increased ventilation of the polluted boundary layer.

Under RCP8.5_2005CH4 (Fig. 4g–i), where methane is held fixed at year 2005 levels, summertime decreases by 2096–2100 are larger (by ~ 4–9 ppb) and winter- and springtime increases smaller (by ~ 8–14 ppb) than under RCP8.5, demonstrating the enhancement of surface MDA8 O_3 concentrations throughout the year by the large CH_4 increases in RCP8.5. Generally changes in MDA8 O_3 throughout all scenarios become larger in the second half of the 21st century.

In Fig. 5 we examine changes across the entire MDA8 O_3 distribution for the early (2021–2025) and late 21st century (2096–2100) relative to the 2001–2005 time period. Under RCP8.5 (Fig. 5a–c), increases occur across the MDA8 O_3 distribution almost year-round in the WE, while we find seasonal differences in both the NE and SE. In summer, decreases in MDA8 O_3 occur at all quantiles, largest at the high tail where MDA8 O_3 decreases by up to 20 ppb in the NE and 35 ppb in the SE. During fall, we also find substantial decreases (up to −27 ppb) across the MDA8 O_3 distribution in the SE. In winter, increases occur at all quantiles in the NE (up to +20 ppb) and SE (up to +11 ppb). There are increases in MDA8 O_3 throughout the distribution in the WE and NE during October-May, with the largest changes (up to 23 ppb) in the upper tail.

Under RCP8.5_WMGG (Fig. 5d–f) the largest increases in MDA8 O_3 in the NE occur during December to February, reaching about +4 ppb from the 30%-quantile throughout the upper tail by the end of the 21st century. Slight decreases occur during late spring and summer, reaching up to −5 ppb at higher quantiles. These decreases in MDA8 O_3 despite climate warming (see Fig. 1) could be a "climate benefit" in regions with consistent decreases across all ensemble members (Figure S4) or may instead reflect climate variability (e.g., Barnes et al., 2016). Rieder et al. (2015) highlight a spatially variable structure of summertime increases in MDA8 O_3 under RCP4.5_WMGG over the NE where largest increases occur along the Eastern Seaboard and at higher latitudes, but ensemble members differ in terms of changes further

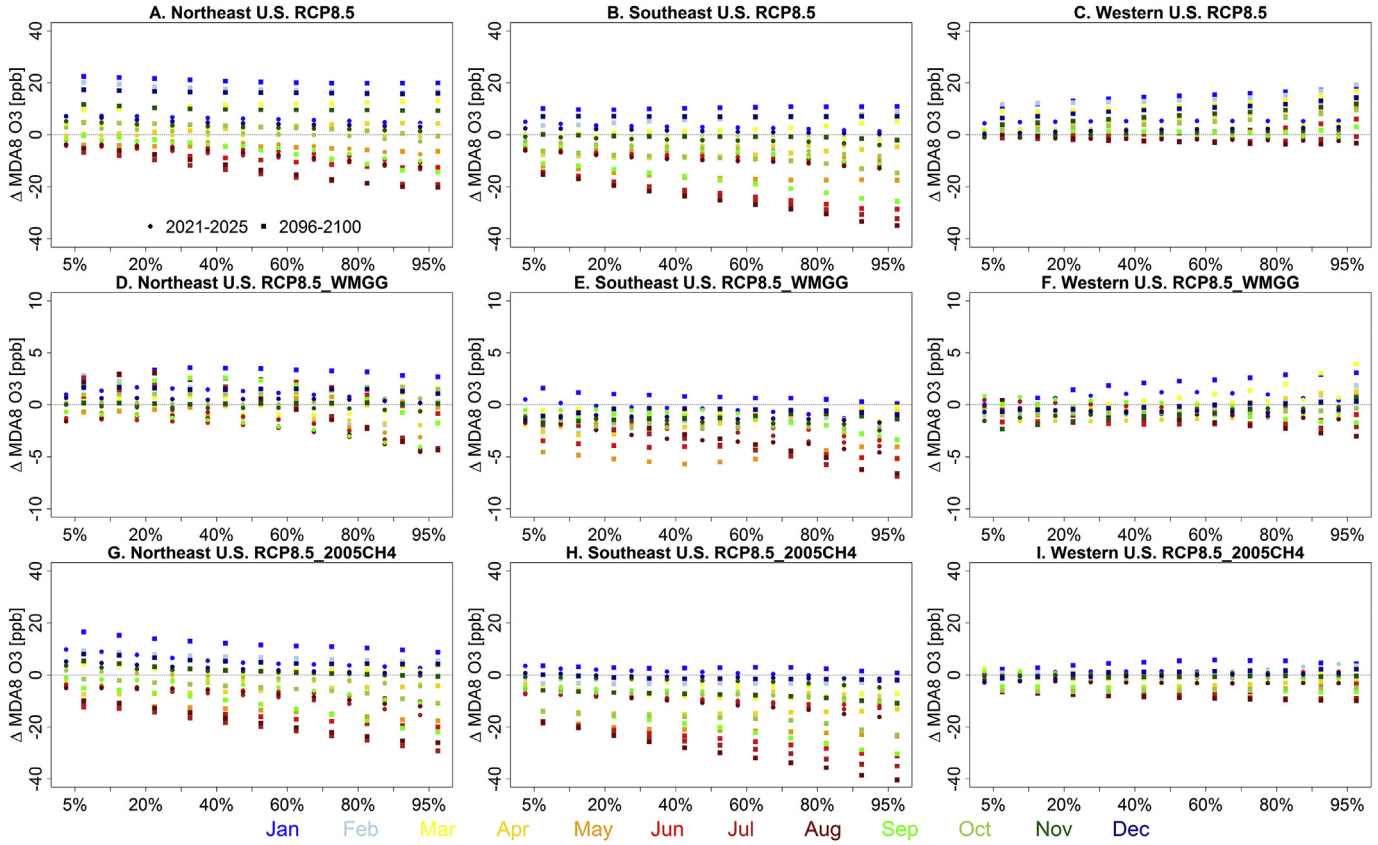

Fig. 5. 3-member ensemble regional average changes in MDA8 O_3 relative to the 2001–2005 base period as projected by CM3 for selected quantiles (5%, 10%, 20%, …, 80%, 90%, 95%) by month (colors) under the RCP8.5 (top), RCP8.5_WMGG (middle) and RCP8.5_2005CH4 (bottom) scenarios for the early (2021–2025) and late (2096–2100) 21st century for three regions: Northeast (left column), Southeast (middle column), Western U.S. (right column). Note, quantile marks are positioned in the middle between the early (circles), and late (squares) period. (For interpretation of the references to color in this figure legend, the reader is referred to the Web version of this article.)

inland. Similar regional patterns as documented in Rieder et al. (2015) for the Eastern U.S. under RCP4.5_WMGG emerge under RCP8.5_WMGG. Results for the WE under RCP8.5_WMGG show slight increases (of up to 4 ppb) in the upper tail of the distribution during January and March, and slight decreases (of up to −3 ppb) throughout summer.

Contrasting RCP8.5_2005CH4 (Fig. 5g–i) vs. RCP8.5 (Fig. 5a–c) highlights a "methane penalty" on MDA8 O_3 over all regions. Across the distribution, MDA8 O_3 decreases are larger (and increases smaller) under RCP8.5_2005CH4, particularly during winter when MDA8 O_3 increases are two to three times smaller than under RCP8.5. The methane penalty under RCP8.5 is particularly pronounced in the WE, leading to a peak-ozone season spanning from December to April by the end of the 21st century. As documented in Clifton et al. (2014) for monthly mean ozone, these changes in seasonality in RCP8.5 primarily reflect methane increases (as demonstrated by the difference between RCP8.5_2005CH4 and RCP8.5). Changes in ozone seasonality manifest also in the seasonal and annual number of days above NAAQS discussed below.

3.2. Projected changes in DAYS > 70 ppb at CASTNet sites

First we focus on 21st century changes in MDA8 O_3 resulting solely from climate warming. With climate warming we find an accompanying increase in DAYS > 70 ppb, respectively, particularly pronounced between late (2096–2100) and early (2021–2025) 21st century in the NE (Fig. 6a and b). Such increases in MDA8 O_3 with increasing surface temperatures have been noted in previous work (e.g., Bloomer et al., 2009, 2010; Fu et al., 2015; Lee et al., 2014; Shen et al., 2016), and are referred to as a "climate penalty" (e.g., Wu et al., 2008).

Contrasting the increases in the number of days above 70 ppb with those of the previous ozone NAAQS (75 ppb, see Figure S5) illustrates the challenge to attain more stringent air quality standards as climate warms in the absence of emission reductions. Around mid-century (2041–2045) 31 out of 38 sites in the NE, 5 out of 10 sites in the SE, 4 out of 13 sites in the WE and 3 out of 4 sites in CA show on average more than 3 exceedances of 70 ppb per year (we note that results for CA are more uncertain as illustrated in Sect. 2). We note that results for RCP4.5_WMGG (see Fig. S6) are similar although slightly weaker than those for RCP8.5_WMGG, despite only half as much warming (Fig. 1).

While initial gains are made in the first few decades of the 21st century due to NO_x emission reductions (Fig. 1a, Table 1), the average number of DAYS > 70 ppb increases in the full RCP8.5 simulation the second half of the 21st century, largest in the WE. Here the number of sites with ≥ 4 DAYS > 70 increases between 2021-2025 and 2096–2100 for a 70 ppb level from 7 to 11 (compare Fig. 6c to d). In the NE and SE, increases in DAYS > 70 are small (during the first half of the 21st century); nevertheless, large-scale exceedances of 70 ppb occur by 2096–2100, particularly for sites in Mid-Atlantic states (Fig. 6d). Overall, the number of NE non-attainment sites increases between 2021-2025 and 2096–2100 from 25 to 29 for a 70 ppb level. These figures highlight that while the NAAQS exceedances in RCP8.5 are somewhat less frequent than in RCP8.5_WMGG (compare Fig. 6a and b with Fig. 6c and d), the reduction is not as great as might be expected given the large NO_x emission reductions alone.

Next we examine the difference between results from the full RCP8.5 simulation and the RCP8.5_2005CH4 simulation, which excludes methane concentration changes. For the majority of CASTNet

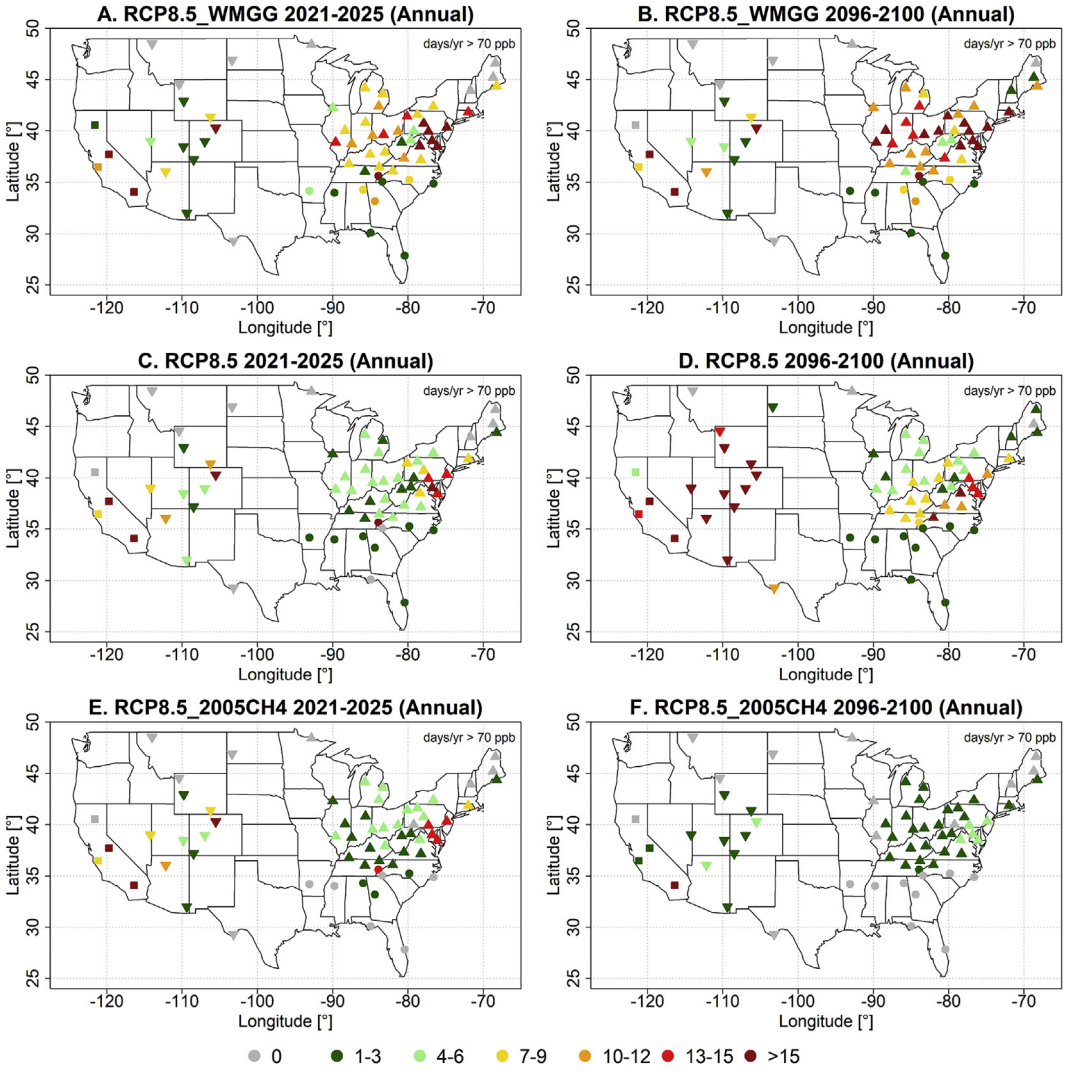

Fig. 6. Projected annual, 3-member ensemble average number of days above 70 ppb for early (2021–2025, left column) and late (2096–2100, right column) 21st century, binned, per CASTNet site for (A–B) RCP8.5_WMGG, (C)–(D) RCP8.5, and (E)–(F) RCP85_2005CH4. For regional symbols see Fig. 1a.

sites, the average number of threshold exceedances under RCP8.5_2005CH4 is by 2096–2100 less than four for a 70 ppb threshold (Fig. 6f). The striking decline in DAYS > 70 ppb (and DAYS > 75 ppb, see Figure S5) in RCP8.5_2005CH4 compared with RCP8.5 (recall the majority of sites shows ≥ 4 days above 70 ppb) implies that the more-than-doubling of global methane abundance from 2005 to 2100 (Fig. 1a, Table 1) contributes significantly to worsening ozone air quality, an effect we refer to as a "methane penalty", i.e. enhanced ozone production resulting from methane oxidation in the presence of NOx. This result is in stark contrast to projections under RCP8.5, highlighting the challenge imposed by rising global methane and the subsequent enhancement of background ozone concentrations for attaining NAAQS levels in the 21st century. With additional model sensitivity simulations (see Figure S7), we confirm that this "methane penalty" arises through chemistry (not the radiative and thus climate effects from methane; see also Clifton et al., 2014).

The net annual change in DAYS > 70 in the individual sensitivity scenarios is attributable to various changes on the seasonal level. Under RCP8.5_WMGG the overall annual increase in Eastern U.S. ozone pollution is mainly driven by summertime increases (Fig. 7a and b), though by the end of the 21st century substantial springtime exceedances of 70 ppb emerge (Fig. 8a and b). This indicates a future seasonal extension of the present-day ozone season, also noted in monthly mean concentrations by Clifton et al. (2014). In the NE 30 sites show more than 3 DAYS > 70 per summer and year by the end of the 21st century, compared to 27 sites in 2021–2025. During spring, exceedances of 3 days per season in 2096–2100 occur at 17 sites, compared to 5 sites in 2021–2025. Changes in fall and winter are smaller. During fall, the number of sites in the NE exceeding 70 ppb at least once per year increases from 23 to 27 from 2021-2025 to 2096–2100. Over the same time period no change in the number of sites exceeding 70 ppb is found for the SE. No site in the WE exceeds 70 ppb during fall.

We show above that substantial exceedances of 70 ppb occur under RCP 8.5 (Fig. 6). These increases mainly occur during spring not summer (compare Fig. 8c and d and Fig. 7c and d), and we attribute them primarily to a chemical "methane penalty".

The seasonal extension of days exceeding threshold concentrations leads to the overall increase in the annual average number of DAYS > 70 under RCP8.5 over the WE and NE and counteracts decreases attained via regional NO_x emission reductions (over 2006–2100, 84% and 83% over the WE and NE, respectively). In contrast, over the SE, the number of summer exceedance days decreases, by up to −9 for the 70 ppb level (Fig. 7). This decline emerges in the second half of the 21st century when NO_x emission reductions outweigh effects of the methane penalty and the climate penalty. At the same time, the methane penalty overtakes the impact of NO_x emission reductions in the SE during spring, leading to up to 6 exceedances of the 70 ppb level.

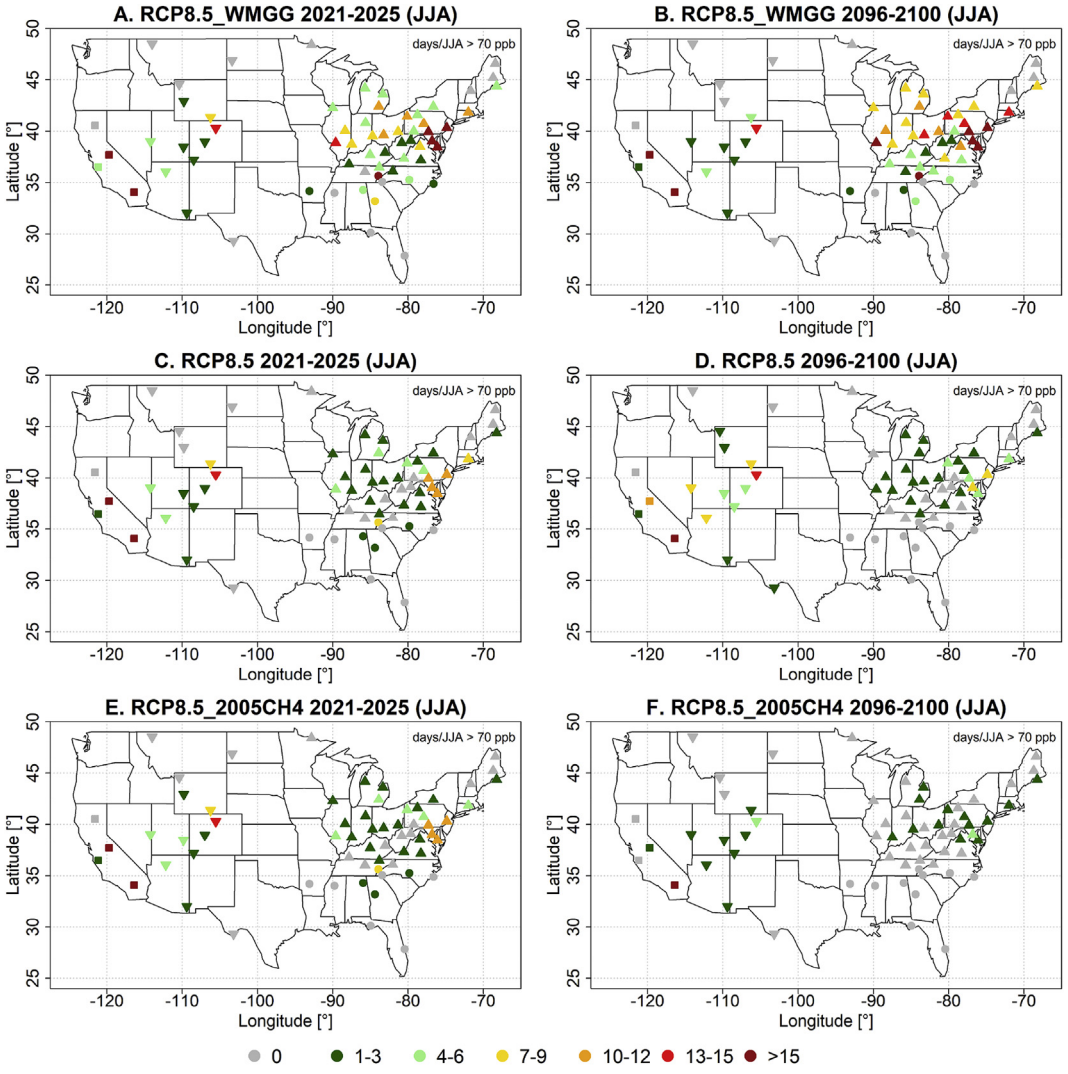

Fig. 7. as Fig. 6 but for summertime (JJA) exceedances only.

Fig. 9 summarizes the seasonal contribution to the regional annual average number of DAYS > 70 for RCP8.5 and RCP8.5_WMGG. Results for the NE and SE under RCP8.5_WMGG highlight the summertime climate penalty in the absence of further NO_x controls. The near doubling of threshold exceedances in the NE and SE for 70 ppb compared to 75 ppb (see Figure S8) indicates that additional efforts in a warming climate will be required to attain air quality targets under more stringent regulations. The methane penalty, emerging in RCP8.5, leads to a strong increase in the number of threshold exceedances during spring and winter despite strong regional NO_x reductions, which manifest mainly in a decreased number of exceedances of the NAAQS during summer season. The resulting shift in the peak ozone season from summer to spring is particularly pronounced in the WE. Here the methane penalty leads to an almost fivefold increase in the number of DAYS > 70 between 2006-2010 and 2096–2100, with almost twice as many exceedances during spring compared to summer. Similar changes, though more muted compared to the WE, occur in the Eastern U.S., with SE exceedances of 70 (and 75) ppb being confined to spring by mid-21st century as RCP8.5 NO_x emission reductions appear sufficient to abate summertime NAAQS exceedances.

3.3. Projected changes in probabilistic MDA8 O_3 return values at CASTNet sites

Fig. 10 shows the annual 4th highest MDA8 O_3 return values (Section 2.2) for the early (2021–2025) and late (2091–2095) 21st century under RCP8.5_WMGG, RCP8.5_2005CH4 and RCP8.5. Contrasting early vs. late 21st century return values under RCP8.5_WMGG, we find a small, robust, increase in the magnitude of return values for the NE (on average 2 ppb), particularly along the Eastern Seaboard (Fig. 10a and b). Return levels elsewhere do not change significantly over the 21st century under this scenario. Similar results are found for RCP4.5_WMGG (Figure S9). Under RCP8.5_2005CH4 (Fig. 10c and d) we find a general decrease in regional return values, ranging between −3 ppb (WE) and −9 ppb (SE) for the early vs. late 21st century. We attribute these changes in RCP8.5_2005CH4 to the strong regional NO_x emission reductions.

By the end of the 21st century, the majority of sites in the WE and NE show probabilistic return values above 70 ppb under RCP8.5, indicating challenges in achieving compliance with the 70 ppb NAAQS level (Fig. 10f). The pronounced increase (6–11 ppb) in the probabilistic MDA8 O_3 return values occurring over the WE under RCP8.5 is mainly attributable to increases in global methane (as determined from the difference between RCP8.5 and RCP8.5_2005CH4). Smaller increases occur over the NE (on average ~ 3 ppb) and SE (on average ~ 1 ppb) as the impact of regional NO_x emission controls largely outweighs effects of climate warming and increasing global methane, compared to the WE. In contrast, under RCP4.5 the majority of sites in both regions shows by the late 21st century (2091–2095) probabilistic MDA8 O_3 return values well below 70 ppb (Figure S9), illustrating improvements

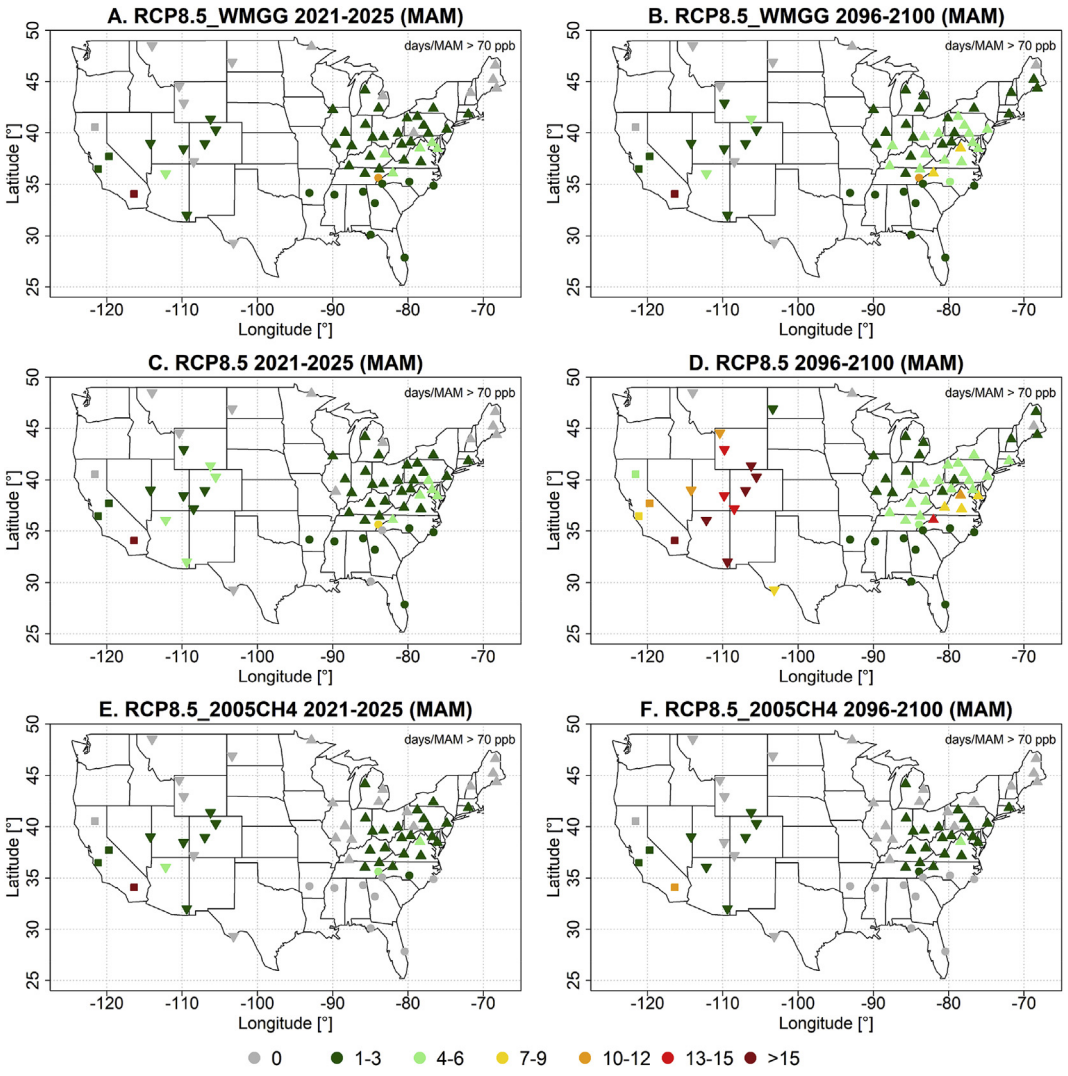

Fig. 8. as Fig. 6 but for springtime (MAM) exceedances only.

in U.S. ambient air quality attainable under an RCP4.5 climate and precursor emission trajectory (see Table 1).

Despite homogeneous regional patterns, by design of our method, differences in the projected 5yr-average 4th highest MDA8 O_3 return values occur among CASTNet sites (Fig. 11). Differences at the site level within a regional domain are explicitly preserved by our statistical transfer method as we assume persistence of local patterns in the future along with a uniform regional change in ozone pollution driven by changes in emissions, climate and/or methane abundances. Under RCP8.5, annual 4th highest MDA8 O_3 return values by 2021–2025 are 55–83 ppb in the NE, 61–78 ppb in the SE, and 56–78 ppb in the WE. By 2091–2095 the values are 62–83 ppb, 62–73 ppb, 65–85 ppb, respectively. Under RCP8.5_WMGG, by the end of the 21st century return values in the Eastern U.S. are slightly higher (59–92 ppb in the NE and 63–83 ppb in the SE). We note that no distinct climate penalty emerges in the WE during the early 21st century though moderate increases in site level return values emerge over time as warming progresses (see also Fig. 1). In contrast probabilistic annual 4th highest MDA8 O_3 return values decline nationwide by −8 to −14 ppb under RCP4.5, with its less extreme warming and limited changes in global methane (see Fig. 1).

Fig. 12 illustrates the temporal evolution of the annual 4th highest MDA8 O_3 return value under RCP8.5, RCP8.5_WMGG and RCP8.5_2005CH4, which reveals the stark differences between changes in the NE vs. WE. While regional average probabilistic return values exceed the present NAAQS level of 70 ppb (and 75 ppb) in the NE under RCP8.5_WMGG starting at 2031–2035 due to the climate penalty, they remain on average below 70 ppb in the WE throughout the 21st century. In contrast, NO_x emission reductions outweigh effects of any climate or methane penalty on the 4th highest return value under RCP8.5 for the NE during the first half of the 21st century, while the methane penalty causes the regional average probabilistic return value in the WE to exceed 70 ppb beginning at 2041–2045 (and 75 ppb at 2071–2075). This spatial dichotomy between the eastern and western parts of the U.S. vanishes in a simulation holding methane fixed (RCP8.5_2005CH4, Fig. 12).

4. Discussion and conclusions

Global chemistry-climate models capture changes in surface ozone most reliably at the regional scale and are not expected to resolve accurately local changes at the site level. Here we describe a novel approach using regional average projections for MDA8 O_3 in the NOAA GFDL global chemistry-climate model CM3 to derive information on changes in ozone levels at individual monitoring sites. Our approach is based on a statistical transfer function relating projected changes for four broad regions to the local monitoring station level (at specific U.S. CASTNet sites) through quantile inflation, which adjusts the observed probability distribution function according to projected changes in the simulated one. 21st century regional average changes at each quantile

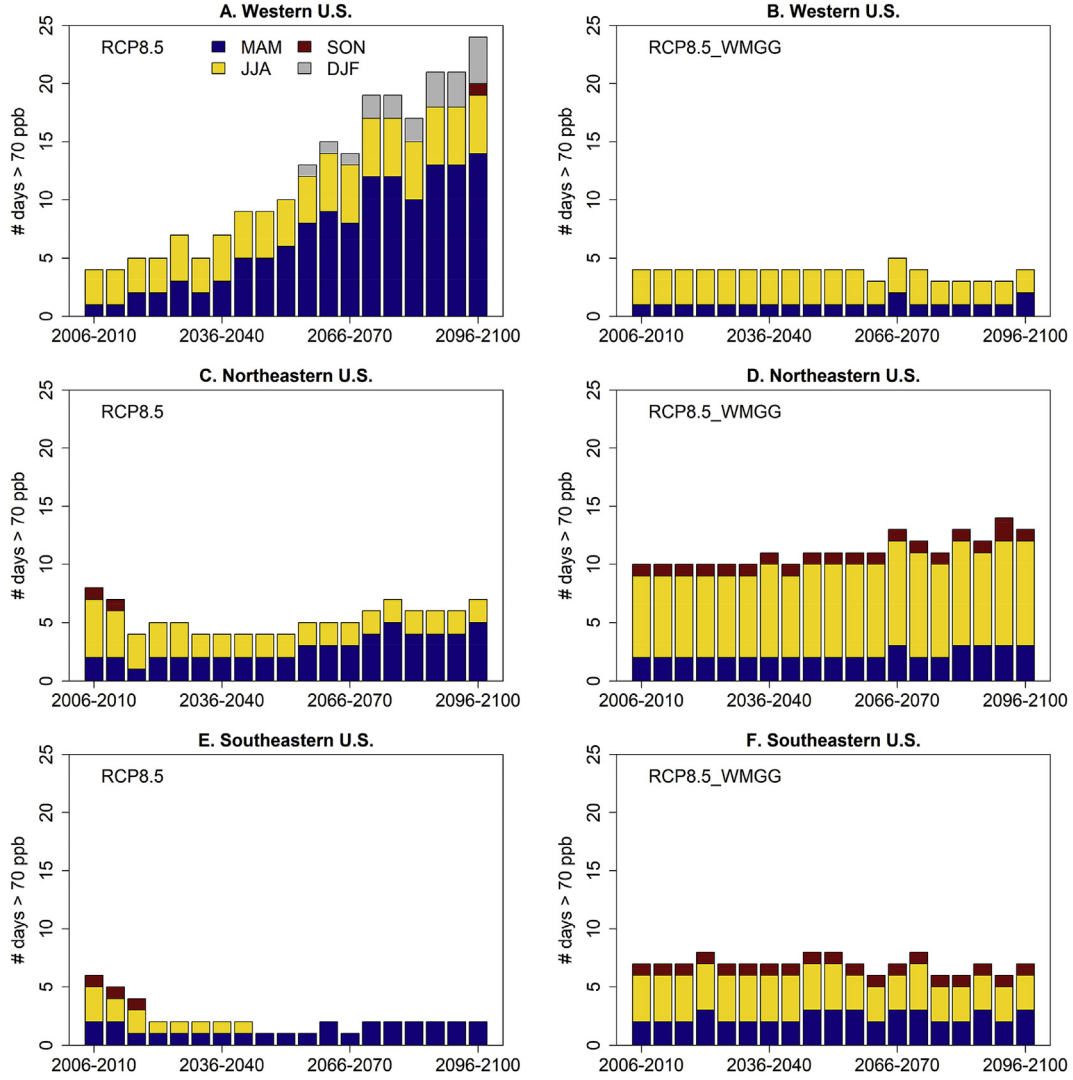

Fig. 9. Average number of days above 70 ppb per region and 5-yr period over the course of the 21st century based on projections under RCP8.5 (left column) and RCP8.5_WMGG (right column) at regional CASTNet sites (see text). Seasonal contributions to the annual average number is indicated by color (see legend in panel (A)). (For interpretation of the references to color in this figure legend, the reader is referred to the Web version of this article.)

from a range of sensitivity simulations are added to observed distributions of MDA8 O_3 at U.S. CASTNet sites. Comparison of the simulated and observed number of days exceeding 70 ppb at individual sites demonstrates the general applicability and robustness of this transfer approach.

Applying this approach to transient simulations with ozone precursor emissions, greenhouse gas concentrations, and methane abundances in a warming scenario (RCP8.5) we find increases in the number of days above 70 ppb between the early and late 21st century. These increases occur, despite strong NO_x emission reductions, particularly in the NE and WE and imply continued challenges to attaining the current NAAQS level under this scenario in which global methane more than doubles. We refer to this increase in ozone via methane oxidation, which emerges during the latter part of the 21st century (see also Clifton et al. (2014)) as a chemical "methane penalty". The effects of this methane penalty offset the beneficial effects of substantial U.S. NO_x emission reductions in RCP8.5; and are particularly pronounced over the WE. Consistent with prior work, we find that climate warming under RCP8.5 with constant year 2005 O_3 precursor emissions leads to a rise in the average number of days where MDA8 O_3 exceeds 70 ppb throughout the 21st century.

While at the beginning of the 21st century the majority of days exceeding 70 ppb occur during summer, strong NO_x emission reductions decrease summertime exceedances over time while the fraction of springtime (and wintertime) exceedances increases under RCP8.5 due to rising methane. The summertime decrease in MDA8 O_3 driven by NO_x emission reductions is most pronounced in the upper tail, but the methane penalty is strongest at the lower tail, with the largest changes in January, likely reflecting a longer ozone lifetime in winter. Such a change in ozone seasonality would have substantial implications for the ozone monitoring season. For example, the strong increase in the annual average number of days above the current 70 ppb U.S. National Ambient Air Quality Standard over the Western U.S., can be largely attributed to springtime MDA8 O_3 increases. In the Western U.S., the number of sites that exceed the 70 ppb level more than 3 times during spring doubles between 2021–2025 and 2041–2045 (4 and 8 sites, respectively) and increases to 11 out of 13 sites by the end of the century, assuming the local differences across sites observed at present is preserved into the future.

We complement frequency based statistics for site level exceedances of 70 ppb with an analysis of probabilistic maximum daily 8-h average ozone (MDA8 O_3) return values. The probabilistic annual 4th highest MDA8 O_3 return values is closely related to the policy-relevant U.S. NAAQS exceedance threshold and bridges the gap to frequency-based statistics as it characterizes the offset relative to the NAAQS by quantifying how close concentrations are to the target threshold.

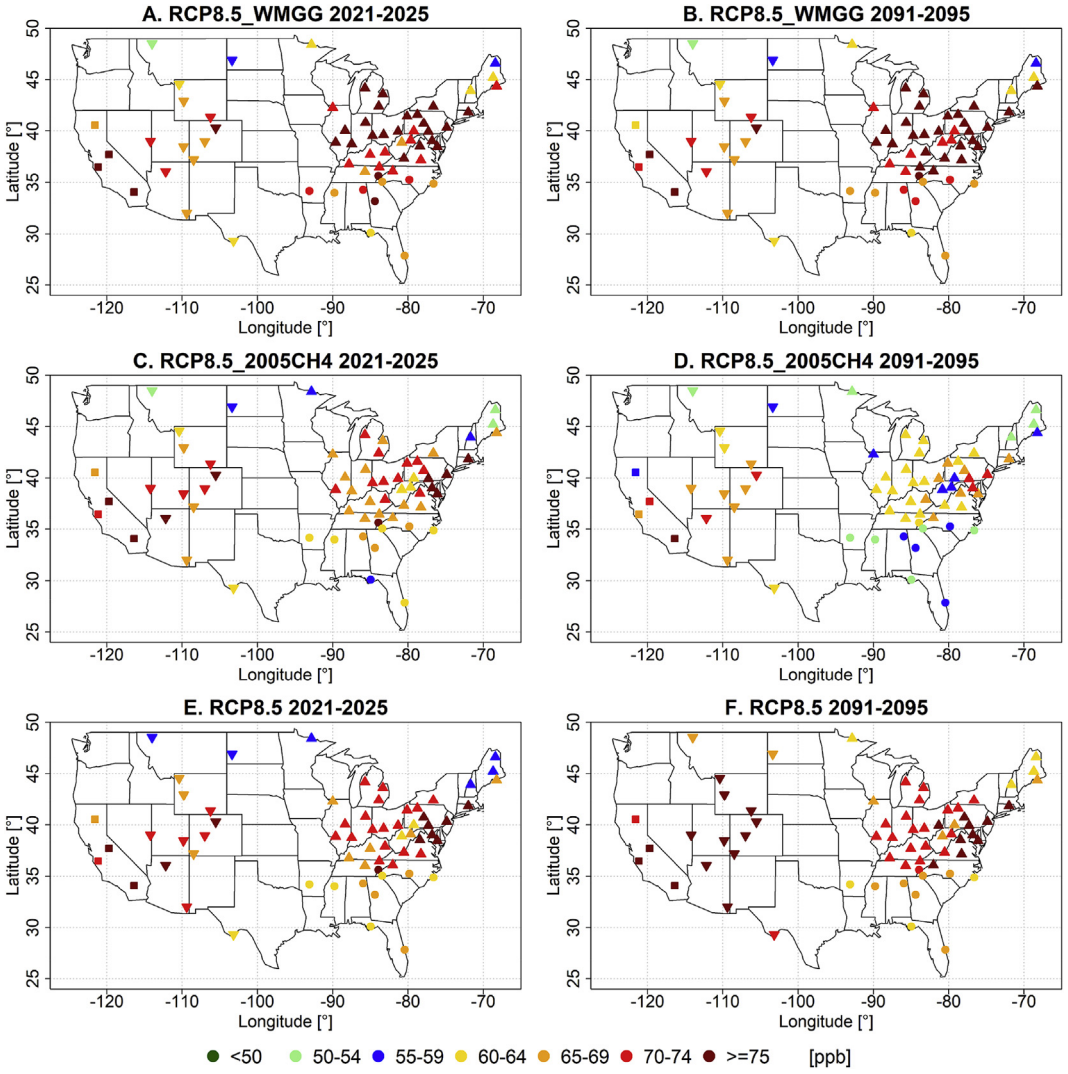

Fig. 10. Projected 3-member ensemble average probabilistic annual 4th highest MDA8 O_3 return value for the early (2021–2025) and late (2091–2095) 21st century under (A–B) RCP8.5_WMGG, (C–D) RCP8.5_2005CH4, (E–F) RCP8.5. For regional symbols see Fig. 1a.

Changes in the probabilistic MDA8 O_3 return values vary strongly across our set of sensitivity simulations. In the absence of ozone precursor emission changes, warming from increases in well-mixed greenhouse gases leads to a small increase in return level magnitude (a climate penalty), particularly over the NE. Probabilistic return values under RCP8.5 vary regionally. While the methane penalty triggers a pronounced increase in surface MDA8 O_3 in the WE, changes are small over the NE and SE where strong NO_x emission controls largely outweigh any increase from climate warming or increasing methane. Nevertheless, the majority of sites across the nation show probabilistic return values above 70 ppb by the end of the 21st century, indicating challenges in achieving compliance with the 70 ppb NAAQS level under RCP8.5, despite strong regional NO_x emission reductions (Table 1). Under RCP4.5, which prescribes only small (−11%) changes in global methane abundances between 2006 and 2100 and substantial NO_x emission reductions of ~80% (see Table 1) the majority of sites show probabilistic MDA8 O_3 return values well below 70 ppb. This effect is particularly visible over the WE and the second half of the 21st century.

Given the continued observed rise in global CH_4 (https://www.esrl.noaa.gov/gmd/ccgg/trends_ch4/) and a potential global shift in the energy sector from coal to natural gas fuel stocks, which may involve higher CH_4 emissions, the potential methane penalty on ozone air quality described here implies a possible disbenefit for attaining U.S. air quality standards. Our analysis harnesses the strengths of a global CCM to provide a first order estimate of site level MDA8 O_3 changes resulting from changes in O_3 precursor emissions, climate warming and rising methane concentrations over the 21st century. Our findings can be used to identify scenarios and time periods that deserve close attention for refined analysis using simulations of computationally more expensive fine-scale regulatory models.

Acknowledgements

This publication was developed under Assistance Agreement No. 835206 and 835878 awarded by the U.S. Environmental Protection Agency. It has not been formally reviewed by EPA. The views expressed in this document are solely those of the authors and do not necessarily reflect those of the Agency. EPA does not endorse any products or commercial services mentioned in this publication. The authors are grateful to two anonymous referees for thoughtful comments on an earlier version of the manuscript.

Appendix A. Supplementary data

Supplementary data related to this article can be found at https://doi.org/10.1016/j.atmosenv.2018.07.042.

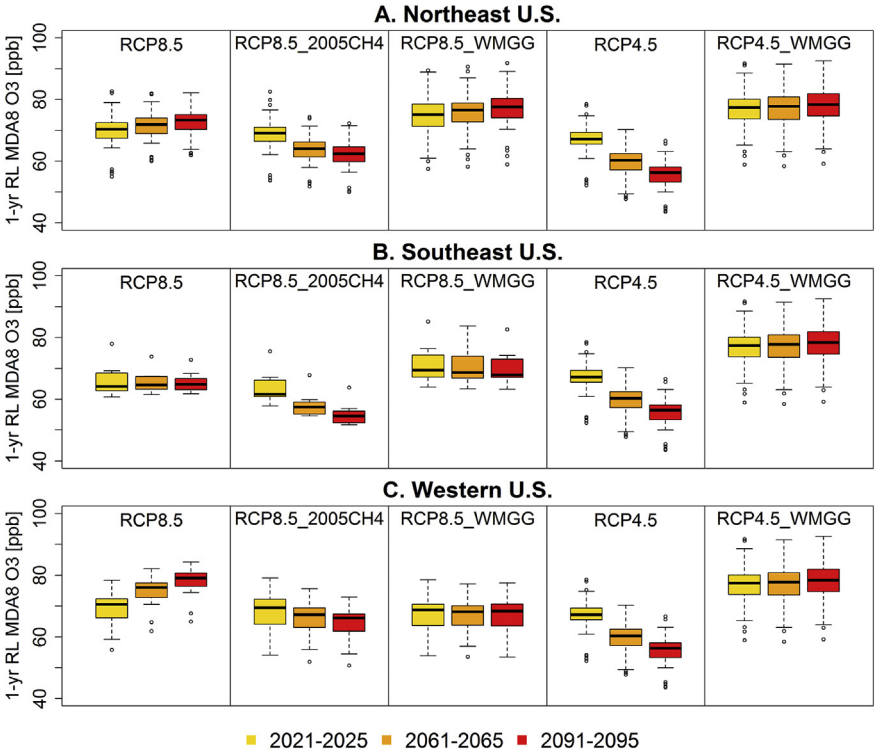

Fig. 11. Boxplot of the regional annual 4th highest MDA8 O_3 return values, averaged over the corresponding ensemble members, at each individual site for the early (2021–2025), mid (2061–2065) and late (2091–2095) 21st century under the RCP8.5, RCP8.5_2005CH4, RCP8.5_WMGG, RCP4.5, and RCP4.5_WMGG scenarios.

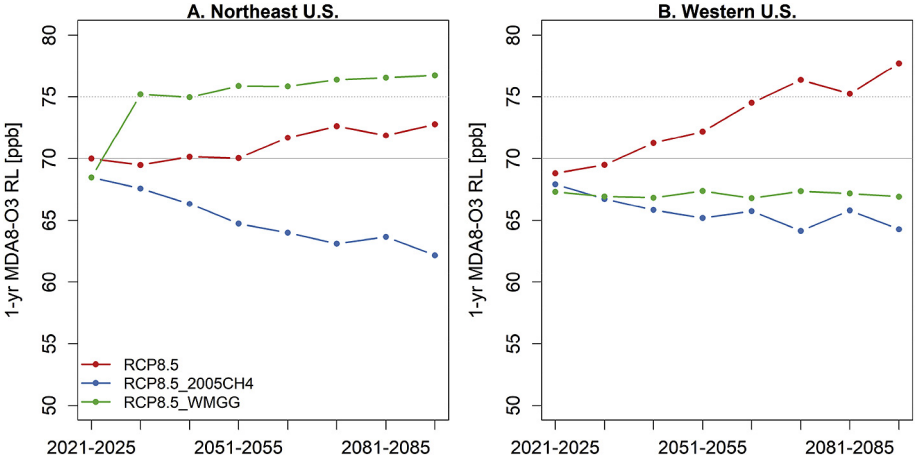

Fig. 12. Temporal evolution of the annual average 4th highest MDA8 O_3 return value across ensemble members under the RCP8.5, RCP8.5_2005CH4 and RCP8.5_WMGG scenarios for (A) the Northeast and (B) the Western U.S. The horizontal grey lines mark the 70 ppb (solid) and 75 ppb (dashed) level.

References

Austin, J., Horowitz, L.W., Schwarzkopf, M.D., Wilson, R.J., Levy, H., 2013. Stratospheric ozone and temperature simulated from the preindustrial era to the present day. J. Clim. 26, 3528–3543.

Barnes, E.A., Fiore, A.M., 2013. Surface ozone variability and the jet position: implications for projecting future air quality. Geophys. Res. Lett. 40, 2839–2844.

Barnes, E.A., Fiore, A.M., Horowitz, L.W., 2016. Detection of trends in surface ozone in the presence of climate variability. J. Geophys. Res.: Atmosphere 121, 6112–6129.

Bloomer, B.J., Stehr, J.W., Piety, C.A., Salawitch, R.J., Dickerson, R.R., 2009. Observed relationships of ozone air pollution with temperature and emissions. Geophys. Res. Lett. 36, L09803.

Bloomer, B.J., Vinnikov, K.Y., Dickerson, R.R., 2010. Changes in seasonal and diurnal cycles of ozone and temperature in the eastern U.S. Atmos. Environ. 44, 2543–2551.

Clifton, O.E., Fiore, A.M., Correa, G., Horowitz, L.W., Naik, V., 2014. Twenty-first century reversal of the surface ozone seasonal cycle over the northeastern United States. Geophys. Res. Lett. 41, 7343–7350.

Coles, S., 2001. An Introduction to Statistical Modeling of Extreme Values. Springer, London.

Cooper, O.R., Langford, A.O., Parrish, D.D., Fahey, D.W., 2015. Challenges of a lowered U.S. ozone standard. Science 348, 1096–1097.

Donner, L.J., Wyman, B.L., Hemler, R.S., Horowitz, L.W., Ming, Y., Zhao, M., Golaz, J.C., Ginoux, P., Lin, S.J., Schwarzkopf, M.D., Austin, J., Alaka, G., Cooke, W.F., Delworth, T.L., Freidenreich, S.M., Gordon, C.T., Griffies, S.M., Held, I.M., Hurlin, W.J., Klein, S.A., Knutson, T.R., Langenhorst, A.R., Lee, H.C., Lin, Y.L., Magi, B.I., Malyshev, S.L., Milly, P.C.D., Naik, V., Nath, M.J., Pincus, R., Ploshay, J.J., Ramaswamy, V., Seman, C.J., Shevliakova, E., Sirutis, J.J., Stern, W.F., Stouffer, R.J., Wilson, R.J., Winton, M., Wittenberg, A.T., Zeng, F.R., 2011. The dynamical core, physical parameterizations, and basic simulation characteristics of the atmospheric component AM3 of the GFDL global coupled model CM3. J. Clim. 24, 3484–3519.

Federal Register, 2008. In: 73 FR 16483-National Ambient Air Quality Standards for Ozone, pp. 16436–16514 Agency, E.P. (Ed.).

Federal Register, 2015. In: 80 FR 65292-National Ambient Air Quality Standards for Ozone, pp. 65292–65468 Agency, E.P. (Ed.).

Fiore, A.M., Jacob, D.J., Field, B.D., Streets, D.G., Fernandes, S.D., Jang, C., 2002. Linking ozone pollution and climate change: the case for controlling methane. Geophys. Res. Lett. 29, 1919.

Fiore, A.M., Naik, V., Leibensperger, E.M., 2015. Air quality and climate connections. J. Air Waste Manag. Assoc. 65, 645–685.

Frost, G.J., McKeen, S.A., Trainer, M., Ryerson, T.B., Neuman, J.A., Roberts, J.M., Swanson, A., Holloway, J.S., Sueper, D.T., Fortin, T., Parrish, D.D., Fehsenfeld, F.C., Flocke, F., Peckham, S.E., Grell, G.A., Kowal, D., Cartwright, J., Auerbach, N., Habermann, T., 2006. Effects of changing power plant NO(x) emissions on ozone in the eastern United States: proof of concept. J. Geophys. Res. Atmos. 111, D12306.

Fu, T.-M., Zheng, Y., Paulot, F., Mao, J., Yantosca, R.M., 2015. Positive but variable sensitivity of August surface ozone to large-scale warming in the southeast United States. Nat. Clim. Change 5, 454–458.

Gao, Y., Fu, J.S., Drake, J.B., Lamarque, J.F., Liu, Y., 2013. The impact of emission and climate change on ozone in the United States under representative concentration pathways (RCPs). Atmos. Chem. Phys. 13, 9607–9621.

Horowitz, L.W., Fiore, A.M., Milly, G.P., Cohen, R.C., Perring, A., Wooldridge, P.J., Hess, P.G., Emmons, L.K., Lamarque, J.F., 2007. Observational constraints on the chemistry of isoprene nitrates over the eastern United States. J. Geophys. Res. Atmos. 112, D12S08.

Horowitz, L.W., Walters, S., Mauzerall, D.L., Emmons, L.K., Rasch, P.J., Granier, C., Tie, X.X., Lamarque, J.F., Schultz, M.G., Tyndall, G.S., Orlando, J.J., Brasseur, G.P., 2003. A global simulation of tropospheric ozone and related tracers: description and evaluation of MOZART, version 2. J. Geophys. Res. Atmos. 108, 4784.

Isaksen, I.S.A., Granier, C., Myhre, G., Berntsen, T.G., Dalsøren, S.B., Gauss, M., Klimont, Z., Benestad, R., Bousquet, P., Collins, W., Cox, T., Eyring, V., Fowler, D., Fuzzi, S., Jöckel, P., Laj, P., Lohmann, U., Maione, M., Monks, P., Prevot, A.S.H., Raes, F., Richter, A., Rognerud, B., Schulz, M., Shindell, D., Stevenson, D.S., Storelvmo, T., Wang, W.-C., van Weele, M., Wild, M., Wuebbles, D., 2009. Atmospheric composition change: climate-Chemistry interactions. Atmos. Environ. 43, 5138–5192.

Jacob, D.J., Winner, D.A., 2009. Effect of climate change on air quality. Atmos. Environ. 43, 51–63.

John, J.G., Fiore, A.M., Naik, V., Horowitz, L.W., Dunne, J.P., 2012. Climate versus emission drivers of methane lifetime against loss by tropospheric OH from 1860-2100. Atmos. Chem. Phys. 12, 12021–12036.

Lamarque, J.F., Bond, T.C., Eyring, V., Granier, C., Heil, A., Klimont, Z., Lee, D., Liousse, C., Mieville, A., Owen, B., Schultz, M.G., Shindell, D., Smith, S.J., Stehfest, E., Van Aardenne, J., Cooper, O.R., Kainuma, M., Mahowald, N., McConnell, J.R., Naik, V., Riahi, K., van Vuuren, D.P., 2010. Historical (1850-2000) gridded anthropogenic and biomass burning emissions of reactive gases and aerosols: methodology and application. Atmos. Chem. Phys. 10, 7017–7039.

Lamarque, J.F., Kyle, G.P., Meinshausen, M., Riahi, K., Smith, S.J., van Vuuren, D.P., Conley, A.J., Vitt, F., 2011. Global and regional evolution of short-lived radiatively-active gases and aerosols in the Representative Concentration Pathways. Climatic Change 109, 191–212.

Lee, Y.C., Shindell, D.T., Faluvegi, G., Wenig, M., Lam, Y.F., Ning, Z., Hao, S., Lai, C.S., 2014. Increase of ozone concentrations, its temperature sensitivity and the precursor factor in South China. Tellus Ser. B Chem. Phys. Meteorol. 66, 1.

Li, J., Mao, J., Fiore, A.M., Cohen, R.C., Crounse, J.D., Teng, A.P., Wennberg, P.O., Lee, B.H., Lopez-Hilfiker, F.D., Thornton, J.A., Peischl, J., Pollack, I.B., Ryerson, T.B., Veres, P., Roberts, J.M., Neuman, J.A., Nowak, J.B., Wolfe, G.M., Hanisco, T.F., Fried, A., Singh, H.B., Dibb, J., Paulot, F., Horowitz, L.W., 2018. Decadal changes in summertime reactive oxidized nitrogen and surface ozone over the Southeast United States. Atmos. Chem. Phys. 18, 2341–2361.

Lin, M., Horowitz, L.W., Cooper, O.R., Tarasick, D., Conley, S., Iraci, L.T., Johnson, B., Leblanc, T., Petropavlovskikh, I., Yates, E.L., 2015. Revisiting the evidence of increasing springtime ozone mixing ratios in the free troposphere over western North America. Geophys. Res. Lett. 42, 8719–8728.

Lin, M., Horowitz, L.W., Payton, R., Fiore, A.M., Tonnesen, G., 2017. US surface ozone trends and extremes from 1980 to 2014: quantifying the roles of rising Asian emissions, domestic controls, wildfires, and climate. Atmos. Chem. Phys. 17, 2943–2970.

Makar, P.A., Staebler, R.M., Akingunola, A., Zhang, J., McLinden, C., Kharol, S.K., Pabla, B., Cheung, P., Zheng, Q., 2017. The effects of forest canopy shading and turbulence on boundary layer ozone. Nat. Commun. 8, 1–14 15243.

Mao, J.Q., Horowitz, L.W., Naik, V., Fan, S.M., Liu, J.F., Fiore, A.M., 2013. Sensitivity of tropospheric oxidants to biomass burning emissions: implications for radiative forcing. Geophys. Res. Lett. 40, 1241–1246.

Meinshausen, M., Smith, S.J., Calvin, K., Daniel, J.S., Kainuma, M.L.T., Lamarque, J.F., Matsumoto, K., Montzka, S.A., Raper, S.C.B., Riahi, K., Thomson, A., Velders, G.J.M., van Vuuren, D.P.P., 2011. The RCP greenhouse gas concentrations and their extensions from 1765 to 2300. Climatic Change 109, 213–241.

Naik, V., Horowitz, L.W., Fiore, A.M., Ginoux, P., Mao, J.Q., Aghedo, A.M., Levy, H., 2013. Impact of preindustrial to present-day changes in short-lived pollutant emissions on atmospheric composition and climate forcing. J. Geophys. Res. Atmos. 118, 8086–8110.

Parrish, D.D., Law, K.S., Staehelin, J., Derwent, R., Cooper, O.R., Tanimoto, H., Volz-Thomas, A., Gilge, S., Scheel, H.E., Steinbacher, M., Chan, E., 2013. Lower tropospheric ozone at northern midlatitudes: changing seasonal cycle. Geophys. Res. Lett. 40, 1631–1636.

Pfister, G.G., Walters, S., Lamarque, J.F., Fast, J., Barth, M.C., Wong, J., Done, J., Holland, G., Bruyère, C.L., 2014. Projections of future summertime ozone over the U.S. J. Geophys. Res. Atmos. 119, 5559–5582.

Rieder, H.E., Fiore, A.M., Horowitz, L.W., Naik, V., 2015. Projecting policy-relevant metrics for high summertime ozone pollution events over the eastern United States due to climate and emission changes during the 21st century. J. Geophys. Res. Atmos. 120, 784–800.

Rieder, H.E., Fiore, A.M., Polvani, L.M., Lamarque, J.F., Fang, Y., 2013. Changes in the frequency and return level of high ozone pollution events over the eastern United States following emission controls. Environ. Res. Lett. 8, 014012.

Shen, L., Mickley, L.J., Gilleland, E., 2016. Impact of increasing heat waves on U.S. ozone episodes in the 2050s: results from a multimodel analysis using extreme value theory. Geophys. Res. Lett. 43, 4017–4025.

Shen, L., Mickley, L.J., Tai, A.P.K., 2015. Influence of synoptic patterns on surface ozone variability over the eastern United States from 1980 to 2012. Atmos. Chem. Phys. 15, 10925–10938.

Simon, H., Reff, A., Wells, B., Xing, J., Frank, N., 2015. Ozone trends across the United States over a period of decreasing NOx and VOC emissions. Environ. Sci. Technol. 49, 186–195.

Steiner, A.L., Tonse, S., Cohen, R.C., Goldstein, A.H., Harley, R.A., 2006. Influence of future climate and emissions on regional air quality in California. J. Geophys. Res.: Atmosphere 111, D18303.

Sun, W., Hess, P., Liu, C., 2017. The impact of meteorological persistence on the distribution and extremes of ozone. Geophys. Res. Lett. 44, 1545–1553.

Trail, M., Tsimpidi, A.P., Liu, P., Tsigaridis, K., Hu, Y., Nenes, A., Russell, A.G., 2013. Downscaling a global climate model to simulate climate change over the US and the implication on regional and urban air quality. Geosci. Model Dev. (GMD) 6, 1429–1445.

Travis, K.R., Jacob, D.J., Fisher, J.A., Kim, P.S., Marais, E.A., Zhu, L., Yu, K., Miller, C.C., Yantosca, R.M., Sulprizio, M.P., Thompson, A.M., Wennberg, P.O., Crounse, J.D., St Clair, J.M., Cohen, R.C., Laughner, J.L., Dibb, J.E., Hall, S.R., Ullmann, K., Wolfe, G.M., Pollack, I.B., Peischl, J., Neuman, J.A., Zhou, X., 2016. Why do models overestimate surface ozone in the Southeast United States? Atmos. Chem. Phys. 16, 13561–13577.

Weaver, C.P., Liang, X.Z., Zhu, J., Adams, P.J., Amar, P., Avise, J., Caughey, M., Chen, J., Cohen, R.C., Cooter, E., Dawson, J.P., Gilliam, R., Gilliland, A., Goldstein, A.H., Grambsch, A., Grano, D., Guenther, A., Gustafson, W.I., Harley, R.A., He, S., Hemming, B., Hogrefe, C., Huang, H.C., Hunt, S.W., Jacob, D.J., Kinney, P.L., Kunkel, K., Lamarque, J.F., Lamb, B., Larkin, N.K., Leung, L.R., Liao, K.J., Lin, J.T., Lynn, B.H., Manomaiphiboon, K., Mass, C., McKenzie, D., Mickley, L.J., O'Neill, S.M., Nolte, C., Pandis, S.N., Racherla, P.N., Rosenzweig, C., Russell, A.G., Salathe, E., Steiner, A.L., Tagaris, E., Tao, Z., Tonse, S., Wiedinmyer, C., Williams, A., Winner, D.A., Woo, J.H., Wu, S., Wuebbles, D.J., 2009. A preliminary synthesis of modeled climate change impacts on US regional ozone concentrations. Bull. Am. Meteorol. Soc., vol. 90, 1843–1863.

Wu, S., Mickley, L.J., Leibensperger, E.M., Jacob, D.J., Rind, D., Streets, D.G., 2008. Effects of 2000–2050 global change on ozone air quality in the United States. J. Geophys. Res. 113, D06302.